Correlation between electrical and mechanical properties in $La_{1-x}Sr_xGa_{1-y}Mg_yO_{3-d}$ ceramics used as electrolytes for solid oxide fuel cells

M. Morales [a,*], J.J. Roa [b], J.M. Perez-Falcón [c], A. Moure [c], J. Tartaj [c], F. Espiell [a], M. Segarra [a]

[a] *Centre DIOPMA, Departament de Ciència dels Materials i Enginyeria Metal$lúrgica, Universitat de Barcelona, Martí i Franquès 1, 08028 Barcelona, Spain*

[b] *CIEFMA, Departament de Ciència dels Materials i Enginyeria Metal$lúrgica, Universitat Politècnica de Catalunya, Avda. Diagonal 647, 08028 Barcelona,*

Spain

[c] *Instituto de Cerámica y Vidrio (ICV-CSIC), Kelsen 5, 28049 Madrid, Spain*

Abstract

The relation between the electrical and the mechanical properties in Sr and Mg doped LaGaO3 ceramics, which can be used as electrolyte for solid oxide fuel cells, was investigated in terms of hardness and ionic conductivity. For this purpose, ceramic materials corresponding to the compositions of La1 - xSrxGa1-yMgyO3-d (LSGM), with x = 0.1 and y= 0.2, and x=0.15 and y =0.2, were prepared. LSGM powders synthesized by the ethylene glycol complex solution method were shaped into disks by isostatic pressing method. The variation in the microstructure of samples was achieved by varying the sintering temperature between 1300 and 1450 ºC. While the effect of the different microstructures on the electrical properties of the LSGM electrolytes was determined by impedance spectroscopy, the influence of the hardness was extracted by instrumented indentation technique. The results showed a linear correlation between the hardness and total ionic conductivity within the temperature range of 500-660 ºC, thus indicating that both properties were strongly influenced on the relative density and purity of the samples. It has a potential practical implication: by measuring the LSGM hardness at room temperature, one can achieve an approach to the ionic conductivity within the studied temperature range.

1. Introduction

Solid Oxide Fuel Cells (SOFCs) are one of the most attractive energy conversion systems, as these devices present a clean energy production, thus promising high efficiencies and low environ- mental impact [1,2]. The electrolyte is one of the key components that decisively control the performance of a SOFC [3]. Among the typical electrolytes, $La_{1-x}Sr_xGa_{1-y}Mg_yO_{3-d}$ (LSGM) is a good candidate to be used as electrolyte for SOFC applications at low and intermediate temperatures, due to that it can achieve ionic con- ductivities as high as 0.166 S cm^{-1} at 800 °C for a composition with $x = 0.20$, and $y = 0.17$ [4,5]. In addition, it exhibits a negligible electronic conductivity at temperatures <1000 °C over a broad range of oxygen partial pressure from pure oxygen ($P(O_2) = 1$ atm) to moistened hydrogen ($P(O_2) = 10^{-22}$ atm) [5,6], and a stable performance over long operating times [7,8]. However, LSGM electrolytes present some problems related to the formation of secondary phases in the grain boundaries, mainly $Sr_3La_4O_9$, LaSr- Ga_3O_7 and $LaSrGaO_4$, which reduce the LSGM conductivity, thus strongly affecting the cell performance [4,9,10]. The typical methods for processing of LSGM are varied: solid state reaction [11,12], steric entrapment synthesis [13], glycine nitrate process [14], and co-precipitation [15], thus usually obtaining values of total conductivities from 0.01 to 0.06 S cm^{-1} at 800 °C.

In addition to high electrical performance, a good mechanical stability must be guaranteed. The determination of hardness (H) is important for evaluating the mechanical performance of materials to be used in practical applications. It is necessary that they with- stand the mechanical stresses during their processing and service. Despite the mechanical requirements, the study of the mechanical properties of LSGM electrolytes has not received much attention. Up to date, only a few studies about mechanical and thermal characterization of Sr and Mg doped $LaGaO_3$ ceramics have been reported in literature, which were mainly performed using macroscopic techniques, such as bending and micro-hardness

tests at different conditions [16e19]. For such reasons, it is essential to determine the mechanical properties of the different LSGM com- positions at the micro/nanoscale using the Instrumented Indenta- tion technique (IIT) [20]. In fact, we have recently reported the mechanical characterization for the $La_{0.85}Sr_{0.15}Ga_{0.8}Mg_{0.2}O_{3-d}$ using this technique [21]. During the last decade, among electrolytes ceramics, lanthanum tungstates, doped ceria, and yttria stabilized zirconia as proton and oxide conducting electrolytes in bulk ma- terial [22e24], thick and thin films [25,26], and multilayered ma- terials [27], have been previously studied by this technique in similar test conditions.

Understanding the correlation between the microstructure, electrical and mechanical properties for LSGM electrolytes is important for both fundamental and application points of view. Up to date, the relations between the microstructure and electrical or mechanical properties in different electrolytes for SOFCs have been studied [22,28]. In other fields of materials, multiple correlations between different functional and mechanical properties have been found [29e31]. However, no detailed work about the correlation between electrical and mechanical behaviour in electrolytes for SOFCs has been reported up to now. It is expected that the possible relations between both properties can be attributed to the electrolyte microstructure, because both electrical and mechanical properties mainly depend on the microstructural factors of elec- trolyte, such as porosity, grain size, vacant density, and presence of impurities [22,28].

In the present work, a correlation between electrical and me- chanical properties in bulk LSGM electrolytes for fuel cells was investigated in terms of ionic conductivity and hardness, thus analyzing the possible relations between them and microstructure. For this purpose, ceramic materials of the compositions of La1—xSrxGa1—yMgyO3—d, x = 0.1 and y = 0.2 (LSGM1020), and x = 0.15 and y = 0.2 (LSGM1520), were prepared at different sintering temperatures between 1300 and 1450 ◦C, and further electrically and mechanically characterized.

2. Experimental procedure

2.1. Material preparation

Ceramic precursors of La0.90Sr0.10Ga0.8Mg0.2O3—d (LSGM1020) and La0.85Sr0.15Ga0.8Mg0.2O3—d (LSGM1520) were obtained by the polymeric organic complex solution method. Aqueous solutions of corresponding nitrates were mixed by stirring with nitric acid (65%) (10 ml) and ethyleneglycol (80 ml) to make a gel. The as obtained solutions were thermally treated in three steps: 80 ◦C for 2 h, 120 ◦C for 3 h to obtain a black resin embedding all the cations, and finally 180 ◦C up to combustion of the polymeric gel previously obtained. After milling in an agate mortar, the resin was calcined at 900 ◦C for 5 h and attrition milled for 2 h in ethanol with ZrO2 ball media. After attrition milling, 0.7 g of the powders were uniaxially pressed in pellets with 0.8 mm diameter at 100 MPa, isostatically pressed at 200 MPa, and finally sintered in air for 12 h at different temperatures (1300, 1350, 1400 and 1450 ◦C) for each composition.

2.2. Material characterization

BET surface area of the powders was determined using a Quantachrome Accusorb instrument. Density of sintered bodies was measured by the Archimedes method with distilled water. The theoretical densities were calculated from the division of the mo- lecular weight by the cell volume calculated by Datta et al. [32], giving values of 6.63 g cm—3 and 6.67 g cm—3 for LSGM1020 and LSGM1520 compositions, respectively. The materials were characterized by X-ray Diffraction (XRD) in a Bruker D8 Advance diffrac- tometer (Cu Ka1 radiation) typically at 3.3$10—2 s—1 scan rate. After polishing and thermal etching, the microstructures of the sintered samples were examined by scanning electron microscopy (SEM) using a Zeiss Microscope (model DSM 950, Germany), which was equipped with an energy dispersive X-ray spectroscopy detector (EDS) to identify the different phases. Finally, the average grain size for both compositions was estimated from image analyses of micrographs.

2.3. Electrical characterization

On each surface of the disk pellets, sintered at different tem- peratures, was painted with an Ag commercial paste (Dupont) to be

used as electrodes. Silver coated pellets were fired at 700 ◦C for 1 h to ensure a good adhesion between the sample surface and silver electrode. Afterwards, the ionic conductivities were measured by an impedance analyser (model HP-4294A, HewlettePackard) in the

frequency range of 10 MHz to 100 Hz at temperatures between 260 and 660 ◦C. The bulk and grain boundary conductivities were

separated as presented in our previous work [35]. Due to the same experimental limitations, it was not possible to carry out mea- surements at temperatures higher than 660 ◦C.

2.4. Mechanical characterization

The pellets were polished with a diamond suspension of decreasing sizes (30, 6, and 3 mm) and finally with colloidal silica in order to obtain a flat surface. The different nanoindentation tests were performed using a Nanoindenter® XP System (Agilent Tech- nologies) equipped with Nanosuite 6.1 application software. The mechanical tests were made by three-sided pyramid Berkovich diamond indenter. The indentation depth curves were continu- ously monitored, and the loadetime history of indentation recor- ded. The shape and the area function of the indenter were calibrated using a fused silica standard with a well-

known Young modulus, 72 GPa [33]. The frame stiffness was automatically corrected and the thermal drift during the experiments was main- tained below 0.05 nm s—1. The different experiments were performed at a penetration depth of 2000 nm. The different H values have been obtained from the correct analysis of loade displacement curves, and employing the Oliver and Pharr method [33]. Each H value presented in this study is an average of 400 measurements performed on four different parts of the same sample in order to achieve statistical significance. Surface obser- vations were performed by atomic force microscopy (AFM), with a Dimension 3100 Microscope (Bruker) working in tapping mode to carry out the different measurements. The image was processed with the WSxM software [34] in order to check the fracture mechanisms activated under indentation stress field.

3. Results and discussion

3.1. Material characterization

Fig. 1 shows the XRD patterns for both LSGM1020 and 1520 compositions sintered at different sintering temperatures. For LSGM1020 ceramic, a single perovskite phase (marked as "0") was observed at the sintering temperatures of 1350 and 1400 ◦C. In contrast, the perovskite phase was only present at a sintering temperature of 1350 ◦C for LSGM1520. Traces of LaSrGaO4 and LaSrGa3O7 as secondary phases were detected in both compositions. Both the LaSrGaO4 and LaSrGa3O7 impurities, which are observed in the clearest and darkest grains, marked as "1" and "2" in Fig. 2, respectively, were also identified by EDSeSEM analysis for some studied microstructures. From the images, it seems to be that while the LaSrGaO4 was mainly located at the grain boundaries, the LaSrGa3O7 was placed at bulk. The results and the aspect of the phases in the micrographs are in agreement with the observed by Lu et al. [9] and in our previous work [35]. In general, the amounts of secondary phases detected by XRD and EDSeSEM in LSGM1520 samples were slightly higher than those of LSGM1020 ones at the same sintering temperatures. The observation of single-phase surfaces with perovskite structure and secondary phases in both the grain boundaries and bulk is a phenomenon previously observed in these compositions by Djurado and Labeau [4].

On the other hand, these microstructures showed that porosity of Sr-rich phase (LSGM1520) is lower than that of LSGM1020, so the increase of Sr content favoured the densification of the ceramics. For the LSGM1020, both relative density and grain size were significantly increased as the sintering temperature approached at 1450 ◦C (Fig. 3). Thus, the relative densities varied from 91.5 to 95.2% for samples sintered between 1300 and 1450 ◦C, respectively. However, the relative densities found for the LSGM1520 sample were not significantly varied (96.1-98.5%) with the sintering temperature. These results are comparable with the results reported by Oncel et al. [36] and Isikawa et al. [37] for single-phase ceramics processed by regenerative solegel and self-propagating high tem- perature synthesis, respectively. These differences in relative den- sity between both compositions may be attributed to that the specific surface area for LSGM1520 powders (9 m2 g—1) was higher than that of LSGM1020 ones (5 m2 g—1). The average grain size for both compositions increased with a similar tendency as the sintering temperature was increased from 1300 to 1450 ◦C. Moreover, the grain size for LSGM1020 at low temperature (1300 ◦C) was smaller than that of Sr-rich composition. The coalescence process of particlesegrains was still not completed at this temperature, which was attributed to the poor sintering ability of the LSGM1020 powders caused by the low specific surface area.

3.2. Electrical properties

Fig. 4 presents the ionic conductivities for both LSGM1020 and LSGM1520 ceramics at different sintering temperatures, determined by impedance spectroscopy in the temperature range of 260-660 ◦C. As shown in Fig. 4a, the highest total conductivities were achieved at sintering temperatures of 1400 and 1350 ◦C for LSGM1020 and 1520 pellets, respectively. They depended mainly on the grain boundary conductivities, which were strongly affected by the sintering temperatures (Fig. 4b and c). For the LSGM1020 composition, the grain boundary conduc- tivities were significantly augmented with increasing the sintering temperature from 1300 to 1400 ◦C. However, they were reduced when the sintering temperature reached 1450 ◦C. A similar tendency was observed in LSGM1520, but the highest grain boundary conductivity was achieved at a lower sintering temperature (1350 ◦C). It indicates a relatively strong presence of secondary phases segregated to the grain boundaries in the samples sintered at the lowest and the highest temperatures, as suggested from XRD and EDSeSEM results. In addition, the dif-

ferences in terms of grain boundary conductivity between the samples of each composition were significantly higher than those in bulk one. It can indicate that, despite the presence of sec- ondary phases in the bulk, the most part of the impurities segregated to the grain boundary.

According to this work, both the relative density and the pres- ence of impure phases should be the main factors that could in- fluence on the ionic conductivities of LSGM. Thus, the ceramics sintered at 1400 ◦C for the LSGM1020 and 1350 ◦C for the LSGM1520 presented the highest total ionic conductivities, which corresponded to the samples with the highest relative densities and without appreciable amounts of secondary phases detected by XRD and EDSeSEM. In addition, the extrapolation of the total ionic conductivities up to 800 ◦C obtained for the samples sintered at 1350 ◦C (LSGM1020) and 1400 ◦C (LSGM1520) indicated that they would be higher than 0.01 S cm—1. The most typical values of total conductivity for LSGM found by other authors vary from 0.01 to 0.06 S cm—1 at 800 ◦C [11e15]. As a result, the electrical properties of the LSGM were comparable to those of samples with different compositions and preparation methods obtained by other authors. Therefore, it indicates the usefulness of these ceramics to be used as an electrolyte for SOFCs. Mechanical properties. Table 1 shows the values of H extracted by IIT for both compo- sitions at different sintering temperatures. In general, the H values obtained for both LSGM1020 and 1520 compositions are much higher than the different values reported by other authors, using conventional techniques, such as micro-hardness. For instance, Baskaran et al. [17] reported hardnesses of 7.0, 7.8 and 8.2 GPa for La0.9Sr0.1Ga0.8Mg0.2O3—d, La0.8Sr0.2Ga0.85Mg0.15O3—d and La0.9Sr0.2Ga0.9Mg0.1O3—d, respectively. This phenomenon is attributed to that the IIT locally measures the mechanical properties, without the influence of the grain size and the different defects mainly generated during the shaping and sintering process. In Fig. 5, an AFM-3D image corresponding to a residual imprint per- formed on the LSGM1020 sintered at 1400 ◦C for an indentation depth of 2000 nm is shown. Generally, high stresses are concen- trated under the contact point between sample and indenter. In this case, several radial cracks have been activated at the corners of the imprints, due to the field stress generated during the indentation process. On the other hand, H values for both compositions were similar to those of gadolinia-doped ceria (GDC, GdxCe1—xO2—x/2 with $0.1 \leq x \leq 0.2$), H = 10.5e11.8 GPa, which were also determined by nanoindentation in a previous work [23]. In contrast,

H for LSGM were lower than those of cubic yttria-stabilized zirconia (YSZ, Y0.08Zr1.92O1.96) that typically presents H = 14e20 GPa [23,24].As expected, the hardness was increased with the relative density for both compositions, except for the LSGM1020 and LSGM1520 samples sintered at T > 1400 ◦C and T > 1350 ◦C, respectively (Table 1). The LSGM1520 ceramics at these temperatures presented high relative densities (96-98%), which were similar to the one sintered at 1350 ◦C, but their H values were much lower (w9 GPa). Therefore, H was decisively affected by the presence of impurities. The significant presence of secondary phases in both the bulk and the grain boundaries, as deduced from the results of both the bulk and grain boundary conductivities, could lead to an easier formation and propagation of cracks in the LSGM1520 ceramics sintered at temperatures different from 1350 ◦C. In particular, the common LaSrGaO4 phase presents low mechanical strength, due to a strong tendency to the cleavage fracture along ab- planes [38]. In contrast, the hardness in the LSGM1020 composition was less influenced by this secondary phase, because it was probably formed in smaller amounts and mainly placed at the grain boundaries, as indicated both the bulk and grain boundary conductivities. In this case, the relative density also significantly affected the hardness at sintering temperatures ≤1400 ◦C, as the differences in porosity were higher than those of LSGM1520. On the other hand, the grain size of the pellets, which strongly depended on the sintering temperature (Fig. 3), could also play an important role in hardness. In the present work, the grain size was enlarged with increasing the sintering temperature, and the hard- ness was also augmented, although this last has no correlation to the grain size, but to the presence of appreciable impurity amounts (Table 1).

3.3. Correlation between ionic conductivity and hardness

From the obtained results for the electrical and mechanical properties, the relation between both properties for both LSGM1020 and LSGM1520 ceramics was studied. In Fig. 6, s/smax ratio as a function of H/Hmax ratio is exhibited at different test temperatures for each sample. Thus, the hardness is represented in normalized terms of the H/Hmax ratio, in which the H corresponds to the hardness value for the different LSGM1020 and LSGM1520 samples at each temperature, and Hmax is the reference hardnessthat corresponds to the highest hardness for each composition that is the sample sintered at 1400 ◦C for LSGM1020 and 1350 ◦C for LSGM1520. On the other hand, the

sample-to-reference total ionicconductivities of each sample (s/smax) were determined from the total ionic conductivities at 500, 600, and 660 ◦C for each sample, and the reference values (smax) also correspond to those of theLSGM1020 and LSGM1520 samples sintered at 1400 and 1350 ◦C, which reached the highest total conductivity. As can be observed inFig. 6, the H/Hmax ratio is linearly correlated with the sample-to-reference total ionic conductivity (s/smax) for all studied samples. That means that the corresponding total ionic conductivity vs. the hardness presents a linear trend within the range of sintering temperature studied for each sample mentioned above. So, the effect of the main microstructural factors, such as the relative density (or porosity) and the absence or relatively significant presence of secondary phases, on both the electrical and the mechanical properties is close. In addition, both the grain boundary conductivity, which determined the total ionic conductivity, and the hardness are more sensitive to the small amounts of impurities than the relative densities. In fact, the influence of the relative density on these properties is only critical when the secondary phases are not detected.

The results presented in this work have a potential practical implication: by measuring the LSGM pellet hardness at room temperature, one can achieve an approach to the ionic conductivity within the studied temperature range. Therefore, this represents an initial and non-destructive way of evaluating the mechanical properties of oxide conducting ceramics, which already provides useful information about the electrical performance through the correlation function shown in Fig. 6. The universality of this rela- tionship to be used in electrolytes of different SOFC designs, such as electrolyte-supported and anode-supported cells, has not been studied yet. However, the LSGM hardness values in bulk form can be employed, as a reference, to compare and determine if a thick film electrolyte of an anode-supported cell presents enough me- chanical quality. So, this correlation may be probably used for any cell design, whether the different phases present in a bulk or thick film electrolyte are homogenously distributed. Then, representative hardness measurements would be obtained by indenting the electrolyte surface, and the ionic conductivity may be estimated from the correlation of both properties. In contrast, secondary phases can be locally formed at the anode-electrolyte interface of an anode-supported cell, due to the high temperature of the cosintering process, especially when a buffer layer based on doped ceria is not used to avoid the chemical reaction between the anode and electrolyte [39]. It strongly decreases the electrical properties in this interface, thus limiting the global performance of the elec- trolyte, which is not detected by

indentation tests performed on the electrolyte surface where the cathode will be deposited later. Therefore, this correlation will be not probably accomplished in these cases. In the future, more work should be done to gain knowledge of these correlations for oxide conducting electrolytes to be used in solid oxide fuel cells and other devices.

4. ConclusionsA linear correlation between electrical and mechanical proper-ties in the La0.90Sr0.10Ga0.8Mg0.2O3—d and La0.85Sr0.15Ga0.8Mg0.2O3—d ceramics, which can be used as electrolytes for solid oxide fuel cells,has been found in terms of hardness and total ionic conductivity within the temperature range of 500e660 ◦C. It has been attributedto that both the electrical and mechanical properties were strongly controlled by the microstructural properties such as the relative density and the presence of both the LaSrGaO4 and LaSrGa3O7 secondary phases. So, highest ionic conductivities and maximum hardness values were obtained in the samples that presented a single perovskite phase (without impurities) and high relative density. In contrast, the samples that exhibited a significant segregation of secondary phases at the grain boundaries led to a strong drop in the hardness and grain boundary conductivity, thus decreasing the total ionic conductivity. Then, these properties were mainly limited by the amount of secondary phases at the grain boundaries. Although the EDSeSEM microstructures of the samples with impurities indicated the presence of these in both the grain boundaries and grains, the results of ionic conductivities evidenced that the most part of the impurities segregated to the grain boundaries. These results presented in this work have a potential practical implication: by measuring the LSGM pellet hardness at room temperature, one can achieve an approach to the ionic conductivity within the studied temperature range (500e660 ◦C), which is close for a practical application in SOFCs.

Acknowledgements

This work was partially funded by the Spanish Government (MAT2011-23623 and UNBA10-4E-316 with co-financing FEDER- EU) and XaRMAE (Xarxa de Referència en Materials Avançats per l'Enginyeria, Generalitat de Catalunya).

References

[1] B.C.H. Steele, A. Heinzel, Nature 414 (2001) 345e352.

[2] US Department of Energy, Office of Fossil Energy, National Energy Technology Laboratory, Fuel Cell Handbook, seventh ed., 2004.

[3] S.M. Haile, Acta Mater. 51 (2003) 5981e6000.

[4] E. Djurado, M. Labeau, J. Eur. Ceram. Soc. 18 (1998) 1397e1404.

[5] T. Ishihara, H. Matsuda, Y. Takita, J. Am. Chem. Soc. 116 (1994) 3801e3803.

[6] P.N. Huang, A. Petric, J. Electrochem. Soc. 143 (1996) 1644e1648.

[7] K.Q. Huang, R.S. Tichy, J.B. Goodenough, J. Am. Ceram. Soc. 81 (1998) 2565e 2575.

[8] J. Yan, H. Matsumoto, M. Enoki, T. Ishihara, Electrochem. Solid-State Lett. 8 (2005) A389eA391.

[9] X.C. Lu, J.H. Zhu, J. Electrochem. Soc. 155 (2008) B494eB503.

[10] M. Morales, J.J. Roa, J. Tartaj, M. Segarra, J. Power Sources 216 (2012) 417e424.

[11] K. Huang, R.S. Tichy, J.B. Goodenough, J. Am. Ceram. Soc. 81 (1998) 2576e 2580.

[12] B. Rambabu, S. Ghosh, W. Zhao, H. Jena, J. Power Sources 159 (2006) 21e28.

[13] Z.-C. Li, H. Zhang, B. Bergman, X. Zou, J. Eur. Ceram. Soc. 26 (2006) 2357e2364.

[14] Y.H. Cho, S.B. Ha, D.S. Jung, Y.C. Kang, J.-H. Lee, Electrochem. Solid-State Lett. 13 (2010) B28.

[15] R. Pelosato, C. Cristiani, G. Dotelli, S. Latorrata, R. Ruffo, L. Zampori, J. Power Sources 195 (2010) 8116e8123.

[16] S. Pathak, D. Steinmetz, J. Kuebler, A. Payzant, N. Orlovskaya, Ceram. Int. 35 (2009) 1235e1242.

[17] S. Baskaran, C.A. Lewinsohn, Y.-S. Chou, M. Qian, J.W. Stevenson,

T.R. Armstrong, J. Mater. Sci. 34 (1999) 3913e3922.

[18] M. Lugovy, V. Slyunyayev, S. Yarmolenko, J. Sankar, T. Graule, J. Kuebler,

D. Nicholson, N. Orlovskaya, Acta Mater. 59 (2011) 4425e4436.

[19] N. Orlovskaya, M. Lugovy, C. Carpenter, S. Pathak, D. Steinmetz, E. Lara-Curzio,

C. Klemenz, M. Radovic, Acta Mater. 57 (2009) 2984e2992.

[20] G.M. Pharr, Mater. Sci. Eng. A 253 (1998) 151e159.

[21] M. Morales, J.J. Roa, J.M. Pérez-Falcón, A. Moure, J. Tartaj, M. Segarra, J. Eur. Ceram. Soc. 32 (2012) 4287e4293.

[22] J.J. Roa, A. Magrasó, M. Morales, P. Núñez, M. Segarra, Ceram. Int. 37 (2011) 1593e1599.

[23] M. Morales, J.J. Roa, X.G. Capdevila, M. Segarra, S. Piñol, Acta Mater. 58 (2010) 2504e2509.

[24] J.J. Roa, J.C. Ruiz-Morales, J. Canales-Vázquez, M. Morales, X.G. Capdevila,

P. Núnez, M. Segarra, Fuel Cells 11 (2011) 124e130.

[25] M. Morales, J.J. Roa, X.G. Capdevila, M. Segarra, S. Piñol, J. New Mater. Electrochem. Syst. 12 (2009) 187e193.

[26] J.J. Roa, E. Gilioli, F. Bissoli, F. Pattini, S. Rampino, X.G. Capdevila, M. Segarra, Thin Solid Films 518 (2009) 227e232.

[27] J.J. Roa, E. Jiménez-Piqué, T. Puig, X. Obradors, M. Segarra, Thin Solid Films 519 (2011) 2470e2476.

[28] M. Khandelwal, A. Venkatasubramanian, T.R.S. Prasanna, P. Gopalan, J. Eur. Ceram. Soc. 31 (2011) 559e568.

[29] B. Fankhänel, E. Müller, T. Fankhänel, W. Siegel, J. Anal. Chem. 361 (1998) 574e576.

[30] S. Sawaya, S. Akita, Y. Nakayama, Nanotechnology 18 (2007) 035702.

[31] E. Bartolomé, J.J. Roa, B. Bozzo, M. Segarra, X. Granados, Supercond. Sci. Technol. 23 (2010) 6, 045013.

[32] P. Datta, P. Majewski, F. Aldinger, J. Alloys Compd 438 (2007) 232e237.

[33] W. Oliver, G.M. Pharr, J. Mater. Res. 7 (1992) 1564e1583.

[34] I. Horcas, R. Fernández, J.M. Gómez-Rodríguez, J. Colchero, J. Gómez-Herrero, A.M. Barom, Rev. Sci. Instrum. 78 (2007) 2668e2677.

[35] A. Moure, A. Castro, J. Tartaj, C. Moure, J. Power Sources 188 (2009) 489e497.

[36] C. Oncel, B. Ozkaya, M.A. Gulgun, J. Eur. Ceram. Soc. 27 (2007) 599e604.

[37] H. Ishikawa, M. Enoki, T. Ishihara, T. Akiyama, J. Alloys Compd 430 (2007) 246e251.

[38] M. Rozumek, R. Majewski, F. Aldinger, K. Kunstler, G. Tomandl, Ceram. Forum Int. 80 (2003) E35eE40.

[39] K.N. Kim, B.K. Kim, J.W. Son, J. Kim, H.W. Lee, J.H. Lee, J. Moon, Solid State Ionics 177 (2006) 2155e2158.

Figure captions

Fig. 1 XRD patterns of: (a) La0.9Sr0.1Ga0.8Mg0.2O3-d; and (b) La0.85Sr0.15Ga0.8Mg0.2O3-d perovskite phases at different sintering temperatures for 12 h. (0, LSGM perovskite; 1, LaSrGaO4; 2, LaSrGa3O7).

Fig. 2 SEM micrographs of LSGM1020 sintered at: (a) 1300ºC; (b) 1350ºC (c) 1400ºC; and (d) 1450ºC, for 12 h; and LSGM1520 sintered at: (e) 1300ºC; (f) and (g) 1350ºC; and (h) 1400ºC, for 12 h. (1, LaSrGaO4; 2, LaSrGa3O7).

Fig. 3 Relative density and grain size as a function of sintering temperature for both LSGM compositions.

Fig. 4 Arrhenius plots of the (a) bulk, (b) grain boundary, and (c) total ionic conductivity of both LSGM1020 and LSGM1520 sintered at different temperatures.

Fig. 5 Hardness as a function of sintering temperature for both LSGM1020 and LSGM1520.

Fig. 6 AFM-3D image of a residual imprint performed on the LSGM1020 sintered at 1400ºC for an indentation depth of 2000 nm.

Fig. 7 Hardness as a function of relative density for both LSGM1020 and LSGM1520 sintered at different temperatures.

Fig. 8 $\sigma/\sigma max$ as a function of H/Hmax for each sample at different temperatures of electrical tests: (a) 573, (b) 673, and (c) 773 K.

Figure 1

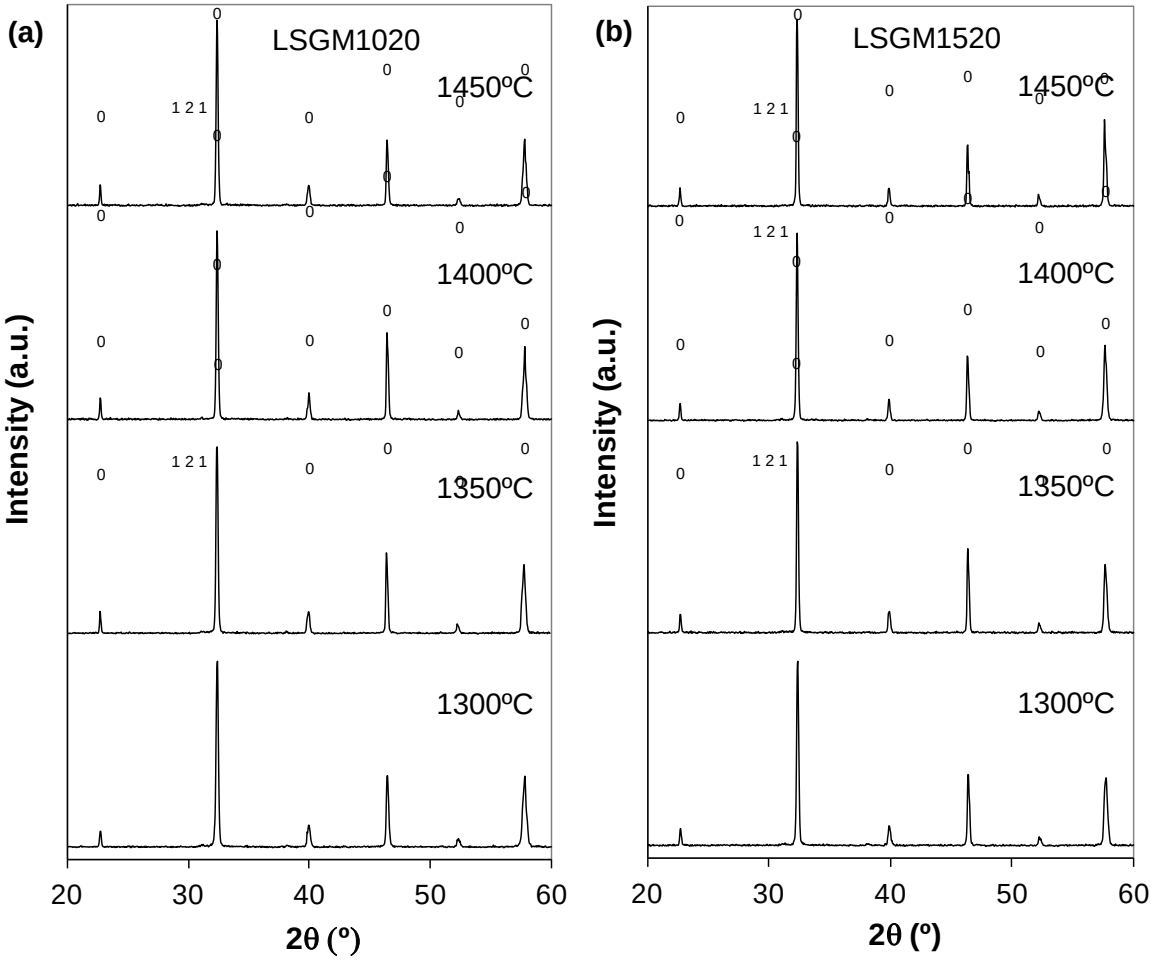
(a)
LSGM1020
1450ºC
1400ºC
1350ºC
1300ºC
121
Intensity (a.u.)
20
30
40
50
60
2θ (º)
(b)
LSGM1520
1450ºC
1400ºC
1350ºC
1300ºC
121
Intensity (a.u.)
20
30
40
50
60
2θ (º)

Figure 2

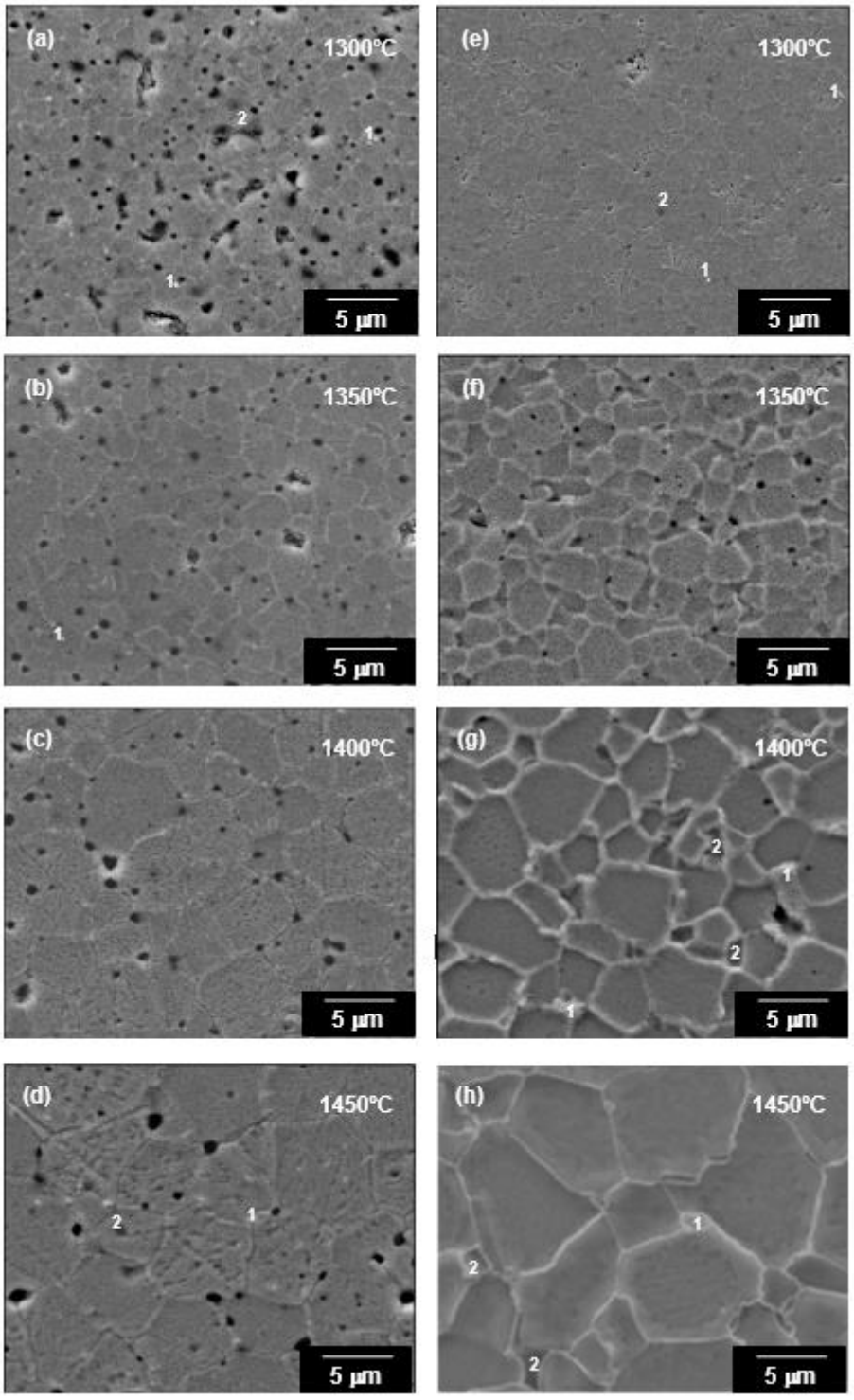
(a)
1300°C
2
1
1
5 µm
(e)
1300°C
1
2
1
5 µm
(b)
1350°C
1
5 µm
(f)
1350°C
5 µm
(c)
1400°C
5 µm
(g)
1400°C
2
1
2
1
5 µm
(d)
1450°C
2
1
5 µm
(h)
1450°C
1
2
2
5 µm

Figure 3

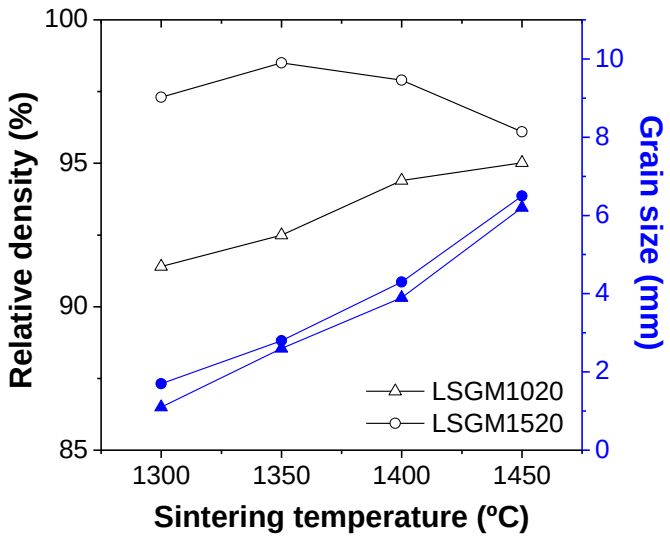

Grain size: □m

Figure 4

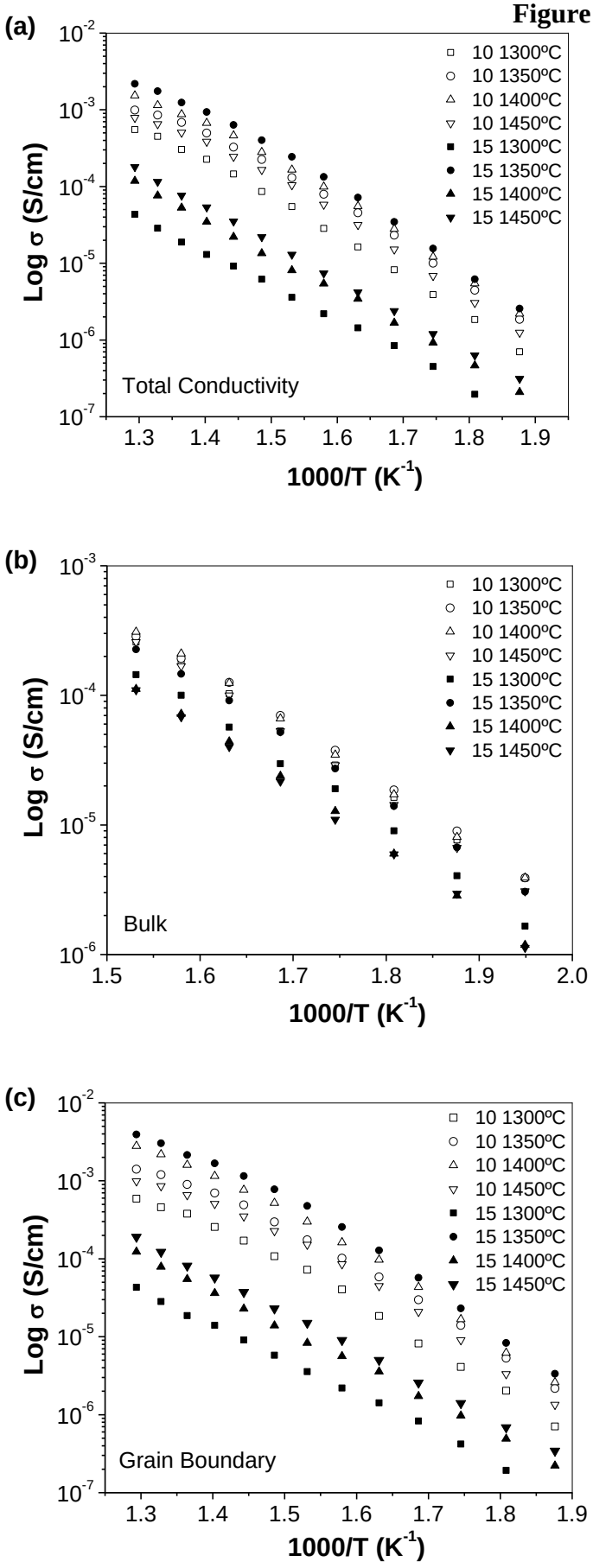
(a)
Log σ (S/cm)
1000/T (K-1)
Total Conductivity
10 1300ºC
10 1350ºC
10 1400ºC
10 1450ºC
15 1300ºC
15 1350ºC
15 1400ºC
15 1450ºC
(b)
Log σ (S/cm)
1000/T (K-1)
Bulk
(c)
Log σ (S/cm)
1000/T (K-1)
Grain Boundary

Figure 5

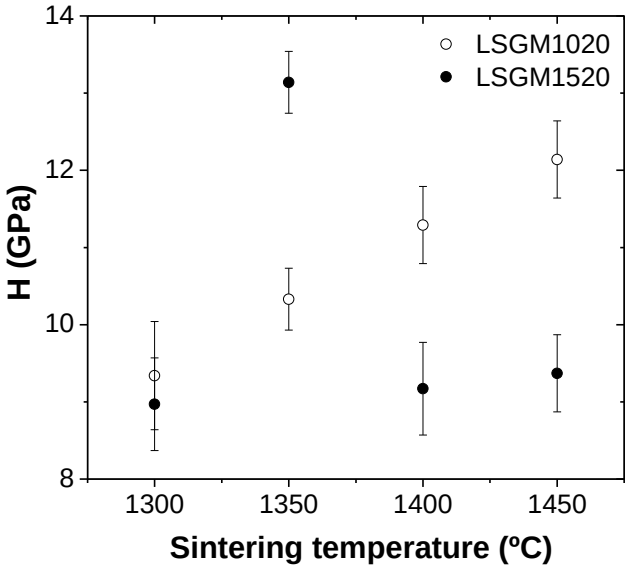
14
12
10
8
H (GPa)
1300
1350
1400
1450
Sintering temperature (ºC)
LSGM1020
LSGM1520

Figure 6

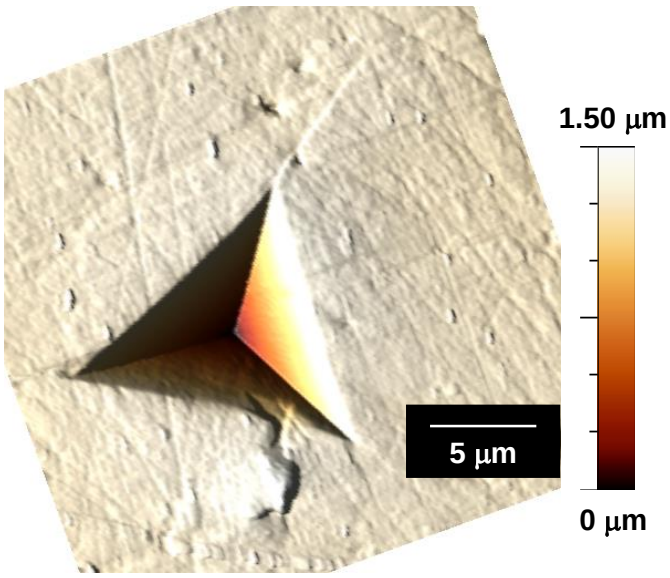

Figure 7

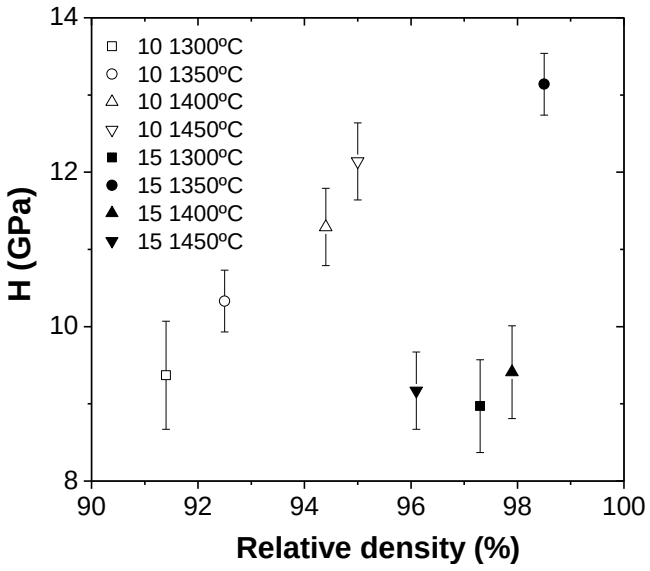
14
12
10
8
90
92
94
96
98
100
H (GPa)
Relative density (%)
10 1300ºC
10 1350ºC
10 1400ºC
10 1450ºC
15 1300ºC
15 1350ºC
15 1400ºC
15 1450ºC

Figure 8

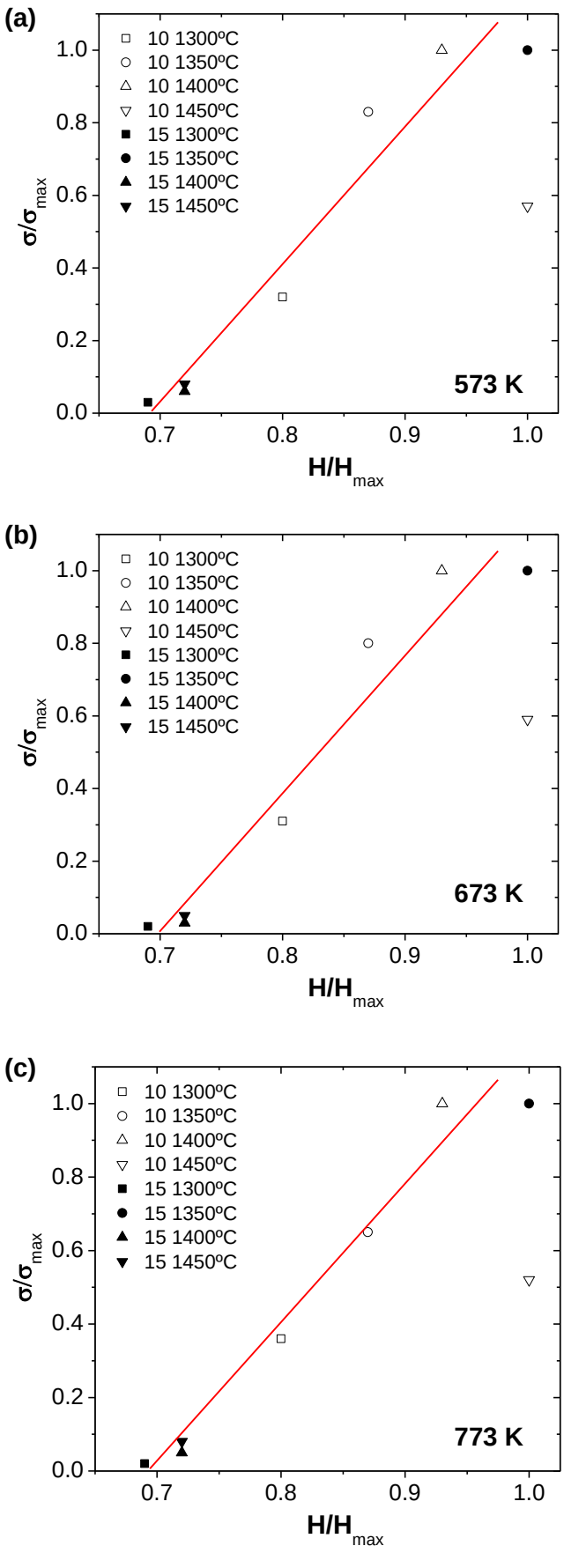
(a)
10 1300ºC
10 1350ºC
10 1400ºC
10 1450ºC
15 1300ºC
15 1350ºC
15 1400ºC
15 1450ºC
573 K
σ/σmax
H/Hmax
(b)
673 K
(c)
773 K